This is a repository copy of *Seed Recipe Design for Batch Cooling Crystallization with Application to l-Glutamic Acid*.

White Rose Research Online URL for this paper:
http://eprints.whiterose.ac.uk/149569/

Version: Accepted Version

# Seed Recipe Design for Batch Cooling Crystallization with Application to L-Glutamic Acid

Fangkun Zhang[a], Tao Liu[a, *], Weixu Chen[a], Cai Y. Ma[b, c], Xue Z. Wang[b, c]

[a] Institute of Advanced Control Technology, Dalian University of Technology, Dalian, 116024, P. R. China

[b] School of Chemical and Process Engineering, University of Leeds, Leeds LS2 9JT, UK

[c] School of Chemistry and Chemical Engineering, South China University of Technology, Guangzhou 510640, China

* Corresponding author. E-mail: tliu@dlut.edu.cn; Tel: +86-411-84706465 Fax: +86-411-84706706

---

**Abstract**: In this paper, a seed recipe design is proposed for batch cooling crystallization to obtain the desired product attributes including product yield and product size distribution, based on simulation studies and experiments on β-L-glutamic acid (β-LGA) crystallization. The impact of seed recipe on product attributes is investigated based on the population balance model (PBM) simulations with respect to the size-dependent growth of crystals. It is found that the product yield is primarily affected by the seed loading ratio (SLR) and the batch time, but less affected by the mean size and variance of seeds. Smaller seeds could improve the product yield and in contrast, larger seeds facilitate the growth into larger crystals but require a larger SLR to ensure the product yield. By introducing an objective function for optimization with the above PBM, a seed recipe design is given for obtaining the desired product attributes as above mentioned. In addition, it is found that washing seeds by the solvent is necessary to ensure seed quality for quantitative seed recipe design and implementation, by comparing three different seed preparation methods. Simulation tests and experiments well demonstrate the effectiveness of the proposed seed recipe design for seeded batch cooling crystallization.

**Keywords:** Seed recipe design, cooling crystallization, population balance model (PBM), batch time, product yield, optimization, L-glutamic acid

---

# 1. Introduction

The seeding technology has been widely applied in industrial crystallization processes for obtaining stable and repeatable products in fine chemicals and pharmaceuticals etc, which could effectively overcome the deficiencies of unseeded crystallizations such as fouling and spontaneous nucleation[1, 2]. It was recognized that seeding has an impact on the product yield and purity, crystal morphology, and crystal size distribution (CSD), which in turn affect the downstream operations such as filtration, drying, and packing of final products[3-5]. Seeded crystallization methods have been increasingly investigated in the past two decades[2, 6-9]. However, for optimization of seeded cooling crystallization processes, the existing literature (see e.g. the references[1, 10-13]) was mainly devoted to the operation conditions of solution temperature, supersaturation, and anti-solvent addition trajectory, rather than seeding. The seed loading, seed quality, and seed size distribution (SSD) were usually considered as uncertainties rather than the control variables for optimizing the product attributes. In fact, it was explored in the references[14, 15] that optimizing the seed recipe design could obtain better effect than optimizing the solution supersaturation for running seeded batch crystallization processes. The recent reference[16] studied the optimization of operation conditions for seeded batch crystallization in terms of different objective functions based on numerical simulations, demonstrating that the seed quality, quantity, morphology, and SSD could play an important role in optimizing the product quality as well as the commonly used solution supersaturation profile.

The seeding conditions mainly consist of seed quality, seed loading ratio (or seed mass) and SSD, which are hereby designated as seed recipe. Since the concept of quality-by-design (QbD) in combination with in-situ process analytical technologies (PATs) has been gradually recognized for crystallization process control and optimization[17, 18], there are increasing studies on design of batch operation conditions including seed recipe in order to obtain crystal products with the desired morphology, CSD, yield, and purity[19, 20]. For batch cooling crystallization processes, the seed recipe and batch time were exemplified as two important operating conditions affecting the product yield and product size distribution (PSD)[21-24]. The seed loading effect on product CSD was investigated by simulations and experiments[22, 25, 26]. In particular, the critical seed loading ratio

to inhibit nucleation was discussed in the references[21, 27, 28]. The effect of seed mass and seed size on product yield and product mean size was investigated based on size-independent growth model simulation[22], demonstrating that increasing the seed mass could increase the product yield while reducing the batch time. The reference[23] studied the effect of seeding in combination with cooling rate and batch time on the final CSD of ammonium sulphate crystallization, revealing that the mean particle size will gradually reach a steady value regardless of seeding, if the batch time is sufficiently long. The impact of seed surface area on the product CSD was investigated in a glycine batch cooling system[25], indicating that the product CSD could be effectively regulated if the seed surface area is over a specific value. It was found by experiments that a proper choice of SLR could result in an unimodal distribution of crystal products[24]. Besides, it was manifested that increasing seed loading ratio (SLR) could effectively decrease the nucleation rate and therefore stabilize the nucleation kinetics during crystallization[26]. The SLR on crystallization kinetics was studied by Huang et al[29], finding that increasing SLR could facilitate the growth kinetics together with a more uniform size distribution of crystal products. The critical SLR for seeded batch crystallization was studied by simulations based on size-independent growth and nucleation model[28], demonstrating that the seed mean size (SMS) takes the most important role in SLR. Concerning the seed recipe design, only a few references were devoted to the optimal design of SLR and SMS[15, 16, 30]. By simulations based on a size-independent growth and nucleation model[15], it was concluded that optimizing the seed size distribution (SSD) could have a larger effect on PSD than optimizing the supersaturation profile. The best objective function for seeded batch crystallization were also studied by simulations based on a size-independent growth model[16], indicating that PSD could be affected by the seed properties more than the supersaturation profile. The references[30] revealed that increasing seed mass while decreasing SMS could effectively reduce the batch time based on model simulations in terms of a constant growth rate.

Note that little result had been explored for quantitative seed recipe design including SMS and SSD to obtain the desired product yield and CSD that are mainly concerned in lots of batch cooling crystallization processes in practice. To address this important issue for practical applications, this paper investigated the effect of seed recipe on the above product attributes,

based on the population balance model (PBM) simulations with respect to the size-dependent growth of crystals. The seeded β-L-glutamic acid (β-LGA) crystallization process is used for case study. By introducing an objective function for optimization with the above PBM, a seed recipe design is given for obtaining the desired crystal product attributes. Simulation tests and experiments are performed to verify the effectiveness of the proposed method.

## 2. Experiments on β-LGA cooling crystallization

### 2.1 Experimental set-up

The experimental set-up is shown in Figure 1, which consists of a 1 L jacketed glass crystallizer, a Pt100 temperature probe, a PTFE four-paddle agitator and a thermostatic circulator (Julabo-CF41). The ATR-FTIR spectroscopy with ReactIR15 software (made by Mettler-Toledo) is utilized to collect the absorbance spectra of LGA solution for measuring the solution concentration. A non-invasive stereo imaging system with a high-resolution camera (made by Pharmavision) is used to monitor the crystal size evolution during crystallization. The camera (UI-2280SE-C-HQ) with a CCD sensor and USB Video Class standard was made by IDS Imaging Development Systems GmbH, which is able to take maximum 6.5 images per second with the pixel resolution of $2448 \times 2050$. The Focused Beam Reflectance Measurement (FBRM) instrument (model G400, made by Mettler-Toledo) is used to measure the number of particles during crystallization in this study. An off-line confocal microscope (Leica DM2500) was used to check the crystal shape information of end-products.

The β-LGA crystals (made by the Sigma Company) with a purity of 99% are taken as the solute, and the distilled water is used as the solvent in this study.

### 2.2 Seed preparation

To obtain high quality seeds for cooling crystallization experiments, three different types of β-LGA seeds were prepared by using different methods of milling, sieving and washing. Table 1 listed the operating conditions used for each method of seed preparation.

The raw β-LGA crystals were milled in a classical mortar for 20 minutes, and then sieved by a sieve shaker (AS 200 digit, produced by Retsch GmbH) for 90 minutes. The sieve sizes from top to bottom were 120 μm, 112 μm, 100 μm, 90 μm, 80 μm, 71 μm, 63 μm, 50 μm, and 40 μm. The β-LGA crystals retained between two sieves with sizes of 71 μm and 80 μm were collected as the seeds for the seeding experiments. The seeds obtained immediately after milling was marked as Seed A. Figure 2 (a) and (d) show the microscopy image of Seed A and its size distribution measured by the above imaging system, respectively. It is seen from Figure 2 (a) that there are a large amount of fine grains, while lots of them are adhered to the surfaces of larger seeds. The phenomenon of a large amount of fine grains in Seed A was further confirmed by the measured seed size distribution shown in Figure 2 (d).

Then the second seed preparation experiment was conducted by taking 5 g Seed A to wash with 75 ml distilled water of 25 ℃ for 3 minutes, so as to dissolve the fine particles. After that, the seed suspension was filtered by a funnel equipped with a filtering paper. The obtained seeds were dried for 24 h under 25 ℃ in a blast type drying oven, and therefore, are marked as Seed B. Figure 2 (b) and (e) show the microscopy image of Seed B and its size distribution measured by the above imaging system, respectively. It is seen that fine grains in Seed B are largely removed. However, there still remain a small amount of fine grains adhered to larger seeds.

Subsequently, the third seed preparation experiment was conducted by taking 5 g Seed A to wash with 150 ml distilled water of 25 ℃ for 3 minutes to remove fine particles. The seed suspension was filtered and dried the same as above to obtain seeds, therefore marked as Seed C. Figure 2 (c) and (f) show the microscopy image of Seed C and its size distribution measured by the above imaging system, respectively. It is observed that fine grains are almost removed from Seed C. Correspondingly, each crystal seed has a clearer shape and smoother surface while following a more uniform size distribution of Gaussian type, compared to Seed A and Seed B.

Three experiments for using the above three types of seeds were conducted based on the experimental setup shown in Figure 1, respectively. The 1 L jacketed glass crystallizer with 500 ml distilled water was first heated up to about 75 °C with a constant stirring speed of 250 rpm in each experiment. Then, 10 g β-LGA crystals were added into the crystallizer for dissolving about

120 min, to guarantee complete dissolution. Subsequently, the solution was cooled down at a cooling rate of 1 °C/min. When it comes to the seeding temperature of 45 °C, 0.6 g crystal seeds of each type were added into the crystallizer, respectively for three experiments. Then, a linear cooling strategy was conducted from 45 °C to 30 °C, totally for 3 h to conduct the crystal growth process. The particle number was measured by FBRM throughout the crystallization process in each experiment.

Figure 3 shows the particle number measured by FBRM and microscopy images of final products from three experiments. It is seen that there is in general an increasing trend of the total particle number after adding each type of seeds. Seed C triggered the smallest number of particles (less than 100) after the addition, whereas the particle number was increased to almost 500 by Seed A. Note that there is obvious fluctuation in counting the particle number for using Seed A. The sharp change from initially about 500 particles to almost 350 particles at the time about 200 seconds is due to that a larger amount of fine grains was dissolved while the remaining larger crystal seeds grow up. For the experiment of using Seed B, the counted particle number was quickly increased to a higher value of 180 compared to the use of Seed C, and then evidently decreased for a while before appearing an increasing trend in common. This phenomenon indicates that there still exist a notable amount of fine grains in Seed B. Besides, it is seen that there is a notable increase of the particle number after 1100 seconds for Seed A and Seed B. This could be provoked by crystal secondary nucleation and breakage owing to rough seed preparation, since Seed C did not result in any notable increase under the same operating conditions. The corresponding microscopy images of final products in Figure 3 also indicate that Seed A and Seed B result in more fine grains and particle agglomerates causing an evident increase of the particle number. Hence, it is necessary to use sufficient solvent to dissolve and/or wash out fine particles in the seeds.

Based on the above experiments for comparing three seed preparation methods, it is concluded that Seed C is the best option for seed preparation. It is also demonstrated that washing seeds by solvent before seeding is necessary to ensure seed quality and quantity for seed recipe design and implementation.

## 3. Simulation model for cooling crystallization and seed recipe

Population balance equations had been widely used for modeling crystallization processes in terms of the first-principles reflecting the mass and energy balance[31]. For seeded batch cooling crystallization, the effect of primary and secondary nucleation may be ignored owing to the fact that the growth process of seeds becomes dominant[22, 32]. So the crystals breakage and agglomeration are also ignored in this study. An one-dimensional PBE for describing the pure growth kinetics of cooling crystallization is generally expressed by

$$\frac{\partial f(L,t)}{\partial t} + \frac{\partial G(L,t) f(L,t)}{\partial L} = 0 \tag{1}$$

where $f(L,t)$ is the number density function that describes the number of crystals with respect to the crystal length and volume of slurry, $t$ the time, $G(L,t)$ the crystal growth rate.

In practice, the growth rate during a cooling crystallization process may be approximately estimated by[33, 34]

$$G(L,S) = k_g S^g (1+\gamma L)^p \tag{2}$$

where $k_g$, $g$, $\gamma$ and $p$ are the model parameters, $S$ is the solution supersaturation defined by

$$S = C(t) - C^*(t) \tag{3}$$

where $C(t)$ and $C^*(t)$ denote the solution concentration and the solution concentration of saturation at the time $t$, respectively. Note that the simplified size dependent growth rate model in (2) has been effectively used for evaluating the product yield and CSD in the references[32, 34, 35].

Generally, the solubility can be estimated by

$$C^* = \alpha_1 T^2 + \alpha_2 T + \alpha_3 \tag{4}$$

where $T$ is the solution temperature, and $\alpha_1$, $\alpha_2$, $\alpha_3$ are the solubility coefficients.

The solute mass balance equation reflects the concentration change along the time evolution, which is in the form of

$$C(t) = C(0) - \rho_c k_v (\mu_3(t) - \mu_3(0)) \tag{5}$$

where $\rho_c$ is the density of crystals in the solution, $k_v$ the volume shape factor, $L$ the characteristic particle size, $f(L,t)$ the number density function, and $\mu_3$ the total volume of crystals that can be estimated by

$$\mu_3(t) = \int_0^\infty L^3 f(L,t)dL \approx \sum_{j=1}^N f_j L_j^3 \Delta L_j \qquad (6)$$

where $N$ denotes the number of discrete points for computation.

The initial and boundary conditions of the above PBE in (1) along with (6) are

$$f(L,0) = f_0(L) \qquad (7)$$

$$f(0,t) = 0 \qquad (8)$$

To solve the above PBE in (1) along with (2)-(8) the high resolution finite volume (HR-FV) method[36] is used herein with respect to $L$.

The seed recipe studied herein include SLR, SMS, and the standard deviation of seed size (SDSS). The SLR is defined as the ratio of seed loading mass to the ideal product mass in theory[28],

$$R_s = \frac{W_s}{W_{th}} \qquad (9)$$

where $W_s$ is the seed mass, $W_{th}$ is the ideal product mass computed by

$$W_{th} = V\left(C_0 - C_f^*\right) \qquad (10)$$

where $C_0$ is the initial solution concentration, $C_f^*$ and $V$ are the saturation concentration and volume of the final solution, respectively.

The SSD denoted by $f_s(L,0)$ is practically assumed to be Gaussian distribution[37] with mean size $\bar{L}_s$ and the standard deviation $\sigma_s$,

$$f_s(L,0) = f_s(L) = \frac{\lambda_s}{\sqrt{2\pi}\sigma_s} \exp\left(-\frac{\left(L - \bar{L}_s\right)^2}{2\sigma_s^2}\right) \qquad (11)$$

where $\lambda_s$ is the seed scaling factor. Note that the assumption of Gaussian distribution could facilitate analyze the effects of SMS and SDSS, respectively, compared to another practical

assumption of log normal distribution where the mean size and variance have cross effect on the distribution properties.

The desired product quality attributes studied herein include the product yield (PY), product mean size (PMS), and the standard deviation of product size (SDPS). The ideal product yield is defined as

$$\text{Yield} = \frac{C_0 - C_f(T)}{C_0 - C_f^*(T)} \times 100\% \tag{12}$$

where $C_f$ and $C_f^*$ are the final solution concentration and the final solution concentration of saturation at the final temperature $T$, respectively.

PMS denoted by the mean of characteristic particle size $\bar{L}_{4,3}$ and SDPS denoted by $\sigma$ are computed by the volume population density function $f_v$ that is estimated by computing the number population density function $f_n$, i.e.,

$$f_{v,i} = \frac{f_{n,i} L_i^3}{\sum\limits_{i=1}^{n} f_{n,i} L_i^3 \Delta L_i} \tag{13}$$

Correspondingly,

$$\bar{L}_{4,3} = \frac{\sum\limits_{i=1}^{n} f_{n,i} L_i^4}{\sum\limits_{i=1}^{n} f_{n,i} L_i^3} \tag{14}$$

$$\sigma = \sqrt{\frac{\int\limits_{0}^{\infty} \left(L - \bar{L}_{4,3}\right)^2 f_v(L,t) dL}{\int\limits_{0}^{\infty} f_v(L,t) dL}} \tag{15}$$

## 4. Investigation of seed recipe for LGA cooling crystallization

To investigate the impacts of SLR, SMS, and SDSS in the seed recipe, respectively, the cooling crystallization of β-LGA is considered here for study. Table 2 lists the crystal growth model parameters of β-LGA estimated for the experimental set-up in Figure 1 by using the

identification method given in the recent paper[34]. The solubility coefficients of β-LGA studied in the reference[33] are used for numerical simulation, which are also listed in Table 2.

Since the desired SLR is generally smaller than 10% for practical application[28], the SLR values from 1.0% to 10% are therefore considered for investigating the impact of seed loading on the above product attributes. The SMS of LGA in a range from 40 to 100 μm are chosen to investigate the seed size effect. The batch time from 1 to 13 h is studied in this work. For each batch, the solution is cooled down from 45 ℃ to 30 ℃ using a linear cooling strategy. Note that the effect of primary and secondary nucleation together with the crystals agglomeration and breakage is neglected as studied in the reference[32], owing to the dominant growth progress of β-LGA seeds. To investigate the growth rate of β-LGA seeds, the initial solution concentration at the seeding temperature is set around the standard saturation concentration to avoid crystal nucleation, e.g., 20 g/L (with respect to the solubility of 18 g/L), and the cooling rate is also taken at a slow level, e.g., smaller than or equal to 0.25 ℃/min, according to the relationship between initial solution concentration, cooling rate and seeding temperature for LGA as discussed in the recent reference[19]. For clarity, the designed operating conditions for simulation are summarized in Table 3.

Based on the above model parameters and operating conditions for PBE in (1) along with (2) -(8), numerical simulations on batch cooling crystallization of LGA are performed to investigate the impacts of SLR, SMS, and SDSS in the seed recipe on the product attributes. Note that the influence from the crystal nucleation, crystal breakage and agglomeration is neglected for the simplicity of analysis. The simulation results are discussed in the following subsections, respectively.

## 4.1 Individual effects of SLR and SMS on the product attributes

Figure 4 shows the product yield with respect to SLR and batch time under a constant seed size distribution like SSD~N(40,15). It is seen that a higher SLR facilitates improving the product yield, but needs a longer batch time for a higher yield.

Figure 5 shows the effect of SMS on the product attributes under a constant SLR like 6% and a constant SDSS like 15 μm. It is seen from Figure 5 (a) that a smaller SMS facilitates improving the product yield, while a higher product yield needs a longer batch time. For instance, the product yield is 65% for an SMS of 40 μm, and in contrast, the product yield is evidently lower for an SMS of 100 μm, about 44%, given the same batch time of 5 h. However, it can be seen that the seed size effect becomes trivial when the batch time is quite long, e.g., 13 h. Figure 5 (b) shows the effects of SMS on the PMS. It is seen that a larger SMS results in a larger PMS. A longer batch time will facilitate growth into larger crystals, but the effect also becomes trivial when the batch time is quite long. Note that not all choices of SMS could obtain the desired PMS even if the batch time is long. For instance, suppose the desired PMS is 150 μm, one hour is enough for taking an SMS of 100 μm, three hour for an SMS of 80 μm seeds, and 7 hour for a SMS of 60 μm, but it is impossible for an SMS of 40 μm under the same operating condition. Figure 5(c) shows the effect of SMS on the SDPS. It is seen that a larger SMS results in a larger SDPS with a sufficient batch time. A longer batch time could broaden the product CSD, but the effect also becomes trivial when the batch time is quite long.

## 4.2 Cross effect of SLR and SMS on the product attributes

Figure 6 shows the cross effect of SLR and SMS on the product attributes under a constant batch time like 3 h and a constant SDSS like 15 μm. It is obviously seen from Figure 6 (a) that there are a common increasing trend on the product yield (solid lines) and a common decreasing trend on the PMS (dashed lines) with respect to SLR. For instance, the product yield is close to 60 % for an SMS of 40 μm but only 38% for an SMS of 100 μm under the same SLR of 10%. In other words, a smaller SMS facilitates improving the product yield owing to a larger amount of seeds under the same SLR. Note that the effect of SLR on the PMS is very limited given the same SMS. For instance, when increasing SLR from 1% to 10%, there is a small decrease of PMS, i.e., from 200 μm to 170 μm given the same SMS of 100 μm.

Figure 6(b) shows the cross effect of SLR and SMS on the SDPS. It is clearly seen that there is a common decreasing trend on SDPS with respect to SLR, i.e., a higher SLR facilitate reducing the SDPS. It is also found that the smaller the SMS, the smaller the SDPS. For instance,

the SDPS is approximately 17.5 μm for an SMS of 40 μm, and increases to almost 19 μm for an SMS of 100 μm under the same SLR of 10%. However, the cross effect of SLR and SMS on reducing the SDPS is very limited.

## 4.3 Cross effect of SLR and SDSS on the product attributes

Figure 7 shows the cross effect of SDSS and SLR on the product attributes under the same SMS and batch time, e.g. 80 μm and 3 h, respectively. It is seen from Figure 7(a) that the product yield increase with respect to SLR (solid lines) as above mentioned, but there is only slight variation with respect to SDSS. This indicates that SDSS has very little effect on the product yield. It is also found that a larger SDSS facilitates the growth into larger crystals. For instance, the PMS is about 140 μm when the SDSS is 5 μm, and increases to almost 155 μm for the SDSS of 20 μm under the same SLR of 10%. However, when compared to SLR, the SDSS brings much less effect to the product yield and PMS.

Figure 7(b) shows the cross effect of SDSS and SLR on the SDPS. It is observed that the SDPS is primarily affected by SDSS, but very slightly affected by SLR. This indicates that the width of the product CSD is primarily affected by the SDSS rather than the crystal growth kinetics. That is to say, a narrow PSD mainly depends on a narrow SSD, which is consistent with the results given in the reference[24].

Based on above analyses and discussions, some conclusions on the impact of seed recipe for batch cooling crystallization of LGA are summarized as follows:

(1) The product yield is primarily affected by SLR along with the batch time, but less affected by SMS and SDSS.

(2) A smaller SMS can improve the product yield given a constant SLR. A larger SMS facilitates the growth into larger crystals, but need a larger SLR to ensure a higher product yield.

(3) The SDPS is primarily affected by SDSS along with the batch time, rather than SLR, SMS or the crystal growth kinetics.

# 5. Seed recipe optimization

Given the desired product attributes in practical applications, e.g., the product yield of 30%, PMS of 170 μm, SDPS of 30 μm, it is expected to design the optimal seed recipe in terms of a suitable batch time for realization. Note that the batch time is usually specified in engineering applications owing to system operation and economic reasons. Based on the above simulation results, a sufficient batch time to obtain the desired product yield can be quantitatively estimated. For example, if the desired product yield is 30%, a sufficient batch time can be roughly estimated from Figure 5(a) as no shorter than 3 h. The seed recipe design is therefore studied based on a specified batch time for system operation, as usually adopted in engineering applications. The following objective function is proposed for optimizing the seed recipe to obtain the desired product attributes,

$$\min_{\theta} \sum_{i=1}^{N} \left( \hat{f}_{v,i} - f_{v,i}^{tar} \right)^2 \tag{16}$$

subject to

$$
\begin{aligned}
& SLR_{min} \leq SLR \leq SLR_{max} \\
& \bar{L}_{min}^{s} \leq \bar{L}_{s} \leq \bar{L}_{max}^{s} \\
& \sigma_{min}^{s} \leq \sigma_{s} \leq \sigma_{max}^{s} \\
& C_{f} \leq C_{f,max}
\end{aligned}
\tag{17}
$$

where $\hat{f}_{v,i}$ and $f_{v,i}^{tar}$ denote the simulated and target volume distributions, respectively. Denote by $\theta = (SLR, \bar{L}_s, \sigma_s)$ the seed recipe vector, by $SLR$ the SLR, by $\bar{L}_s$ the SMS (μm), by $\sigma_s$ the SDPS (μm).

For the case study of batch cooling crystallization of LGA, the constraints in (18) are taken as $SLR \in (0.02, 0.1)$, $\bar{L}_s \in (40, 100)$ and $\sigma_s \in (10, 30)$. The constraint $C_f \leq C_{f,max}$ is determined by the ideal product yield in (12). The operating conditions for seed recipe optimization are the same with the above model simulation as shown in Table 3. In view of that the constrained optimization in (16) and (17) is a constrained nonlinear programming problem, the sequential quadratic programming (SQP) approach in the MATLAB optimization toolbox is adopted to solve the optimal seed recipe. The main steps for seed recipe optimization are summarized as follows.

**Seed recipe optimization algorithm**

---

**Step 1**: Initialize the seed recipe vector $\theta_0 = (0.06, 70, 20)$, and define the step sizes of seed recipe variables, e.g., $\Delta SLR = 0.01$, $\Delta L = 1\mu m$, and $\Delta\sigma = 1\mu m$ for LGA crystallization, respectively.

**Step 2**: Use the HR-FVM method[36] to solve the PBE in (1) along with (2)-(8) for estimating the product volume distribution $\hat{f}_v$ in (13).

**Step 3**: Solve (16) and (17) using the SQP method via the 'fmincon' function in the MATLAB optimization toolbox, and check if the iteration is convergent or not. If not, go to next step. Otherwise, go to Step 5.

**Step 4**: Update the values of seed recipe variables by increasing the step sizes, respectively, and return to Step 2 by letting $k = k + 1$.

**Step 5**: Compute the product mean size and size variance using (14) and (15), and output the optimal seed recipe denoted by $\theta_k$.

---

Using the above seed recipe optimization algorithm, the optimal result is listed in Table 4. Consequently, numerical simulation based on the PBE in (1) is performed to verify if the optimized seed recipe could realize the desired product attributes. The simulation results are shown in Table 5. It is seen that the simulated product attributes are close to the target product attributes, well demonstrating that the desired product attributes can be quantitatively predicted by the proposed seed recipe design based on numerical simulation.

## 6. Experimental verification

To verify the above simulation results for seeded batch cooling crystallization of LGA, a seeded cooling crystallization experiment was performed, by using the same operating conditions listed in Table 3. The batch time is taken as 3 h. According to the above optimized seed recipe, the seeds for experimental verification were prepared using the seed preparation method for Seed

C, which is also listed in Table 4, along with the relative errors to the computed optimum for reference.

Figure 8 shows a snapshot of the prepared seeds measured by the in-situ imaging system shown in Figure 1, and a comparison between the measured SSD and the optimized SSD indicated by SMS and SDSS in Table 4. By observing 2473 particles among the prepared seeds using the above in-situ imaging system, it was verified that the size distribution of these seeds is approximately normal distribution as shown in Figure 8(b). Note that the image analysis method developed in the recent paper[38] was adopted to measure the lengths of these particles. In Figure 8(b), the optimized SSD marked in red corresponds to the optimal SMS and SDSS computed by the above seed recipe optimization algorithm; the blue histogram shows the measured size distribution of the prepared seeds by using the above imaging system for the seed suspension; the computed SSD marked in green is a fitting result in terms of the mean size and size variance of the measured SSD. From Table 4 and Figure 8, it is seen that the SLR can be precisely prepared according to the optimized SLR, but there exists a small error between the measured SSD and the optimized SSD, due to the seed preparation and measurement errors. Nevertheless, the prepared seed recipe is close to the optimized seed recipe, which are therefore used for experiment verification.

The experiment was performed the same as those in Section 4.2. After the experiment, the product suspension was discharged from the crystallizer outlet. After filtering, drying and weighting, the product yield computed by the solid products was 32%. Figure 9 shows an offline microscopy image of the final crystal products.

Figure 10 shows the measured solution concentration during the seeded cooling crystallization process in comparison with the simulation result based on the optimal seed recipe, while the particle number is measured by FBRM for reference. Note that the in-situ measurement of solution concentration was conducted by the ATR-FTIR spectroscopy in terms of the spectral calibration method[39] that could guarantee the prediction accuracy of solution concentration based on the metastable zone data for spectral model calibration. It is seen that the initial values of measured and simulated solution concentrations are close to each other, owing to the fact that the

solution was initially supersaturated (no increase in concentration) at the time of seeding. At the end of the experiment, the measured and simulated concentrations were also close to each other, indicating the similar product yields. Besides, it is also seen from Figure 10 that there is a small decrease of the measured particle number after adding seeds, indicating very little fine grains contained in the prepared seeds and therefore demonstrating the advantage of the proposed seed preparation. Then, a slight increase of the particle number is observed along the time evolution, which may arise from crystal secondary nucleation and breakage. This is a reason causing the errors between the experimental results and simulation results only based on the seed growth model.

Figure 11 shows the CSD dynamic evolution of the PBE in (1) and its projection onto the plane of crystal mean size with respect to the time, based on the optimized seed recipe. It is seen that the volume of SSD increases with the time evolution, indicating that the crystal seeds gradually grow into the desired PSD. Figure 11(b) shows that the PSD is broadened along with the increase of crystal size. This is in accordance with the results shown in Figures 5(b) and (c) that the PMS and SDPS increase with respect to the batch time, well demonstrating the effectiveness of the above simulation based on the size-dependent growth model in (1) for representing the crystal growth dynamics.

Figure 12 shows a comparison between the target, simulated, and measured PSDs in terms of volume percentages of different sizes of final products. It is seen that the simulated PSD based on the optimal seed recipe is very close to the target PSD, while the measured PSD is also close to the target PSD with small errors. Table 5 lists a comparison of the final product attributes. It is seen that the simulated product attributes are very close to the target product attributes, with the relative errors below 5%. This demonstrates that the desired product attributes can be effectively predicted by model-based simulation. Moreover, the measured product attributes from the experiment are also close to the simulated and target product attributes, with a bit larger relative errors. These errors may arise from imprecise seed recipe preparation as shown in Table 4 and measurement error in the experiment. Note that the measured SDPS appears a larger deviation, i.e., 12.3%, which was likely provoked by the prepared seeds due to the relative error of 8.0%

shown in Table 4. This is in accordance with the conclusion made in Section 4 that the SDPS is primarily affected by SDSS.

## 7. Conclusions

A seed recipe design has been proposed for obtaining the desired product attributes including product yield and product size distribution, based on simulation studies and experiments on batch cooling crystallization of β-LGA. The individual and cross effects of SLR, SMS and SDSS on the product attributes were analyzed, respectively. It is therefore concluded that the product yield is primarily affected by SLR and the batch time for seeded batch cooling crystallization. With a specified SLR, smaller seeds can improve the product yield. In contrast, larger seeds facilitates the growth into larger crystals, but require a larger SLR to ensure a higher product yield. Accordingly, a seed recipe design is given for obtaining the desired product attributes, by introducing an objective function to the size-dependent growth model of PBM. Simulation results based on the PBM of LGA demonstrate that the desired product yield and PSD can be quantitatively conducted by the proposed seed recipe design. Experiments on seeded cooling crystallization of β-LGA verify the effectiveness of the proposed seed recipe design for practical application. In addition, a good seed preparation method is proposed to ensure the seed quality for seed recipe design and implementation, which stresses the necessity to wash seeds by the solvent. Note that there appears a bit larger relative error of SDPS in the experimental result compared with that of the simulation result. This could be caused by using the simplified growth model for seed recipe design without considering other crystallization mechanisms such as crystal dissolution, secondary nucleation and breakage, which deserves a further study to reduce the error in the future work.

## Acknowledgement

## A list of abbreviations

| | |
|---|---|
| ATR-FTIR | Attenuated total reflection-Fourier transform infrared spectroscopy |
| CSD | Crystal size distribution |
| FBRM | Focused beam reflectance measurement |
| HR-FVM | High resolution-finite volume method |
| LGA | L-glutamic acid |
| PBM | Population balance model |
| PMS | Product mean size |
| PSD | Product size distribution |
| SDSS | Standard deviation of seed size |
| SDPS | Standard deviation of product size |
| SLR | Seed loading ratio |
| SMS | Seed mean size |
| SQP | Sequential quadratic programming |
| SSD | Seed size distribution |

# References

(1) Nagy, Z. K.; Fevotte, G.; Kramer, H.; Simon, L. L., Recent advances in the monitoring, modelling and control of crystallization systems. Chemical Engineering Research & Design 2013, 91(10), 1903-1922.

(2) Yu, Z. Q.; Chew, J. W.; Chow, P. S.; Tan, R. B. H., Recent advances in crystallization control an industrial perspective. Chemical Engineering Research and Design 2007, 85(7), 893-905.

(3) Ni, X.; Liao, A., Effects of mixing, seeding, material of baffles and final temperature on solution crystallization of L-glutamic acid in an oscillatory baffled crystallizer. Chemical Engineering Journal 2010, 156(1), 226-233.

(4) Ulrich, J.; Jones, M. J., Seeding technique in batch crystallization, in: A. Chianese, H.J.M. Kramer (Eds.), Industrial crystallization process monitoring and control, Wiley-VCH Verlag GmbH, Weinheim, Germany, 2012, 127-138.

(5) Coles, S.; Threlfall, T. L., A perspective on a century of inert seeds in crystallisation. CrystEngComm 2014, 16(21), 4355-4364.

(6) Hu, Q.; Rohani, S.; Jutan, A., Modelling and optimization of seeded batch crystallizers. Computers & Chemical Engineering 2005, 29(4), 911-918.

(7) Mesbah, A.; Huesman, A. E. M.; Kramer, H. J. M.; Nagy, Z. K., Real-time control of a semi-industrial fedbatch evaporative crystallizer using different direct optimization strategies. AIChE Journal 2011, 57(6), 1557-1569.

(8) Flood, A. E.; Srisanga, S., An improved model of the seeded batch crystallization of glucose monohydrate from aqueous solutions. Journal of Food Engineering 2012, 109(2), 209-217.

(9) Wang, H.-Y.; Ward, J. D., Seeding and optimization of batch reactive crystallization. Industrial & Engineering Chemistry Research 2015, 54(38), 9360-9368.

(10) Hanaki, K.; Nonoyama, N.; Yabuki, Y.; Kato, Y.; Hirasawa, I., Design of constant supersaturation cooling crystallization of a pharmaceutical: A simple approach. Journal of Chemical Engineering of Japan 2007, 40(1), 63-71.

(11) Lindenberg, C.; Martin Krattli, J.; Mazzotti, M., Design and optimization of a combined cooling/antisolvent crystallization process. Crystal Growth & Design 2009, 9(2), 1124-1136.

(12) Srinivasan, K.; Dhanasekaran, P., Nucleation control and crystallization of L-glutamic acid polymorphs by swift cooling process and their characterization. Journal of Crystal Growth 2011, 318(1), 1080-1084.

(13) Hemalatha, K.; Nagveni, P.; Naveen, P.; Rani, K. Y., Multiobjective optimization and experimental validation for batch cooling crystallization of citric acid anhydrate. Computers & Chemical Engineering 2018, 112, 292-303.

(14) Aamir, E.; Nagy, Z. K.; Rielly, C. D., Optimal seed recipe design for crystal size distribution control for batch cooling crystallisation processes. Chemical Engineering Science 2010, 65(11), 3602-3614.

(15) Chung, S. H.; Ma, D. L.; Braatz, R. D., Optimal seeding in batch crystallization. The Canadian Journal of Chemical Engineering 1999, 77(3), 590-596.

(16) Hsu, C. W.; Ward, J. D., The best objective function for seeded batch crystallization. AIChE Journal 2013, 59(2), 390-398.

(17) Thirunahari, S.; Chow, P. S.; Tan, R. B. H., Quality by design (QbD)-based crystallization process development for the polymorphic drug tolbutamide. Crystal Growth & Design 2011, 11(7), 3027-3038.

(18) Simon, L. L.; Pataki, H.; Marosi, G.; Meemken, F.; Hungerbuhler, K.; Baiker, A.; Tummala, S.; Glennon, B.; Kuentz, M.; Steele, G.; Kramer, H. J. M.; Rydzak, J. W.; Chen, Z. P.; Morris, J.; Kjell, F.; Singh, R.; Gani, R.; Gernaey, K. V.; Louhi-Kultanen, M.; O'Reilly, J.; Sandler, N.; Antikainen, O.; Yliruusi, J.; Frohberg, P.; Ulrich, J.; Braatz, R. D.; Leyssens, T.; von Stosch, M.; Oliveira, R.; Tan, R. B. H.; Wu, H. Q.; Khan, M.; O'Grady, D.; Pandey, A.; Westra, R.; Delle-Case, E.; Pape, D.; Angelosante, D.; Maret, Y.; Steiger, O.; Lenner, M.; Abbou-Oucherif, K.; Nagy, Z. K.; Litster, J. D.; Kamaraju, V. K.; Chiu, M. S., Assessment of recent process analytical technology (PAT) trends: a multiauthor review. Organic Process Research & Development 2015, 19(1), 3-62.

(19) Zhang, F.; Liu, T.; Huo, Y.; Guan, R.; Wang, X. Z., Investigation of the operating conditions to morphology evolution of β-L-glutamic acid during seeded cooling crystallization. Journal of Crystal Growth 2017, 469(1), 136-143.

(20) Hemalatha, K.; Ran, K. Y., Multiobjective optimization of unseeded and seeded batch cooling crystallization processes. Industrial & Engineering Chemistry Research 2017, 56(20), 6012-6021.

(21) Kubota, N.; Doki, N.; Yokota, M.; Sato, A., Seeding policy in batch cooling crystallization. Powder Technology 2001, 121(1), 31-38.

(22) Patience, D. B.; Dell'Orco, P. C.; Rawlings, J. B., Optimal operation of a seeded pharmaceutical crystallization with growth-dependent dispersion. Organic Process Research & Development 2004, 8(4), 609-615.

(23) Hojjati, H.; Rohani, S., Cooling and seeding effect on supersaturation and final crystal size distribution (CSD) of ammonium sulphate in a batch crystallizer. Chemical Engineering and Processing 2005, 44(9), 949-957.

(24) Yu, Z. Q.; Chow, P. S.; Tan, R. B., Seeding and constant-supersaturation control by ATR-FTIR in anti-solvent crystallization. Organic Process Research & Development 2006, 10(4), 717-722.

(25) Lung-Somarriba, B. L. M.; Moscosa-Santillan, M.; Porte, C.; Delacroix, A., Effect of seeded surface area on crystal size distribution in glycine batch cooling crystallization: a seeding methodology. Journal of Crystal Growth 2004, 270(3), 624-632.

(26) Long, B. W.; Yang, H. T.; Ding, Y. G., Impact of seed loading ratio on the growth kinetics of mono-ammonium phosphate under isothermal batch crystallization. Korean Journal of Chemical Engineering 2016, 33(2), 623-628.

(27) Doki, N.; Yokota, M.; Sasaki, S.; Kubota, N., Size distribution of needle-shape crystals of monosodium L-glutamate obtained by seeded batch cooling crystallization. Journal of Chemical Engineering of Japan 2004, 37(3), 436-442.

(28) Tseng, Y. T.; Ward, J. D., Critical seed loading from nucleation kinetics. AIChE Journal 2014, 60(5), 1645-1653.

(29) Huang, D.; Liu, W.; Zhao, S.; Shi, Y.; Wang, Z.; Sun, Y., Quantitative design of seed load for solution cooling crystallization based on kinetic analysis. Chemical Engineering Journal 2010, 156(2), 360-365.

(30) Zhang, D. J.; Liu, L. D.; Xu, S. J.; Du, S. C.; Dong, W. B.; Gong, J. B., Optimization of cooling strategy and seeding by FBRM analysis of batch crystallization. Journal of Crystal Growth 2018, 486, 1-9.

(31) Fujiwara, M.; Nagy, Z. K.; Chew, J. W.; Braatz, R. D., First-principles and direct design approaches for the control of pharmaceutical crystallization. Journal of Process Control 2005, 15(5), 493-504.

(32) Ma, C. Y.; Wang, X. Z., Model identification of crystal facet growth kinetics in morphological population balance modeling of L-glutamic acid crystallization and experimental validation. Chemical Engineering Science 2012, 70, 22-30.

(33) Hermanto, M. W.; Kee, N. C.; Tan, R. B.; Chiu, M. S.; Braatz, R. D., Robust bayesian estimation of kinetics for the polymorphic transformation of L‐glutamic acid crystals. AIChE Journal 2008, 54(12), 3248-3259.

(34) Guan, R.; Liu, T.; Zhang, F.; Huo, Y., Optimal control of L-glutamic acid crystal size distribution based on population balance model. Chinese Journal of Chemical Engineering 2017, 68(3), 956-963.

(35) Ochsenbein, D. R.; Schorsch, S.; Salvatori, F.; Vetter, T.; Morari, M.; Mazzotti, M., Modeling the facet growth rate dispersion of β-L-glutamic acid—Combining single crystal experiments with nD particle size distribution data. Chemical Engineering Science 2015, 133, 30-43.

(36) Gunawan, R.; Fusman, I.; Braatz, R. D., High resolution algorithms for multidimensional population balance equations. AIChE Journal 2004, 50(11), 2738-2749.

(37) Hermanto, M. W.; Braatz, R. D.; Chiu, M. S., High-order simulation of polymorphic crystallization using weighted essentially nonoscillatory methods. AIChE Journal 2009, 55(1), 122-131.

(38) Huo, Y.; Liu, T.; Liu, H.; Ma, C. Y.; Wang, X. Z., In-situ crystal morphology identification using imaging analysis with application to the L-glutamic acid crystallization. Chemical Engineering Science 2016, 148(12), 126-139.

(39) Zhang, F.; Liu, T.; Wang, X. Z.; Liu, J.; Jiang, X., Comparative study on ATR-FTIR calibration models for monitoring solution concentration in cooling crystallization. Journal of Crystal Growth 2017, 459(1), 50-55.

# Tables and Figures

Table 1. Comparison of different methods of seed preparation.

| Process condition | Seed A | Seed B | Seed C |
|---|---|---|---|
| Milling | ✓ | ✓ | ✓ |
| Milling time | 20 min | 20 min | 20 min |
| Sieving | ✓ | ✓ | ✓ |
| Sieving time | 90 min | 90 min | 90 min |
| Sieve size | 71-80 μm | 71-80 μm | 71-80 μm |
| Seed mass | 5.0 g | 5.0 g | 5.0 g |
| Dissolving solvent | - | water | water |
| Water volume | - | 75 ml | 150 ml |
| Dissolving time | - | 3 min | 3 min |
| Filtering | - | ✓ | ✓ |
| Drying time (h) | - | 5 | 5 |

Table 2. Model parameters for simulation study.

| Variables | Name | Value | Units |
|---|---|---|---|
| $k_g$ | Growth parameter | 6.251 | $\mu m \cdot s^{-1}$ |
| $g$ | Growth parameter | 1.595 | - |
| $\gamma$ | Growth parameter | 0.00893 | $\mu m^{-1}$ |
| $p$ | Growth parameter | 1.85 | - |
| $\alpha_1$ | Solubility coef. | $7.644 \times 10^{-3}$ | g/L |
| $\alpha_2$ | Solubility coef. | -0.1165 | g/L |
| $\alpha_3$ | Solubility coef. | 6.622 | g/L |

Table 3. Operating conditions for simulating batch cooling crystallization of LGA.

| Operating condition | Value | Units |
|---|---|---|
| Seed loading ratio | 1% -10% | - |
| Seed mean size | 40-100 | μm |
| Seed standard deviation | 5-20 | μm |
| Seeding solution concentration | 20 | g/L |
| Seeding temperature | 45 | °C |
| Final solution temperature | 30 | °C |
| Solute density | 1.54 | g/cm$^3$ |
| Solvent mass | 1000 | g |
| Shape factor | 0.031 | - |
| Batch time | 2-14 | h |
| Cooling mode | Linear | |

Table 4. Comparison between the computed and prepared seed recipes.

| Seed recipe | SLR | SMS | SDSS |
|---|---|---|---|
| Computed optimum | **6.4%** | **79 μm** | **25 μm** |
| Experiment preparation | **6.4%** | **77 μm** | **27 μm** |
| Relative error | 0 | **2.5%** | **8.0%** |

Table 5. Comparison of the final product attributes.

| Product attributes | PY | PMS | SDPS |
|---|---|---|---|
| Target | 30% | 170 μm | 30 μm |
| Simulation result | 31% | 172.4 μm | 31.3 μm |
| Experimental result | 32% | 178.6 μm | 33.7 μm |
| Relative error of the simulated result | 3.3% | 1.4% | 4.3% |
| Relative error of the experimental result | 6.7% | 5.1% | 12.3% |
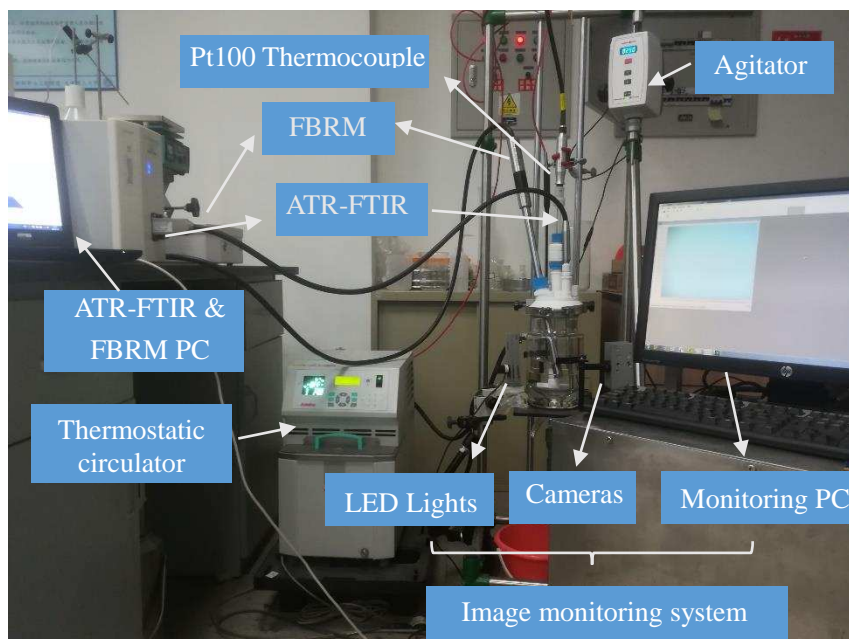
Figure 1. Experimental set-up for in-situ measurement.
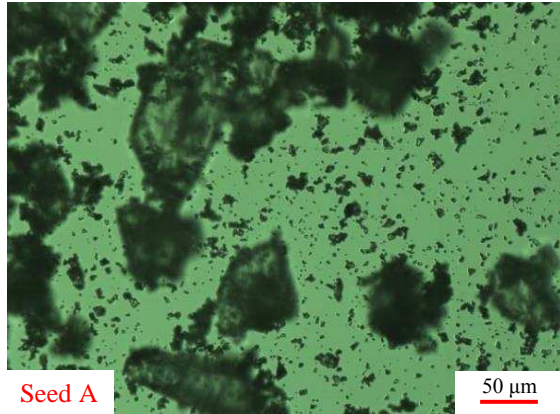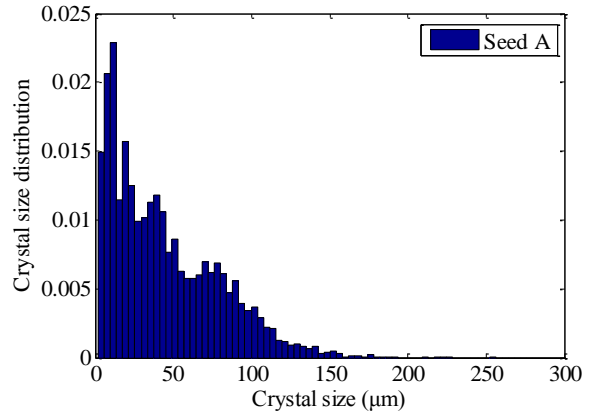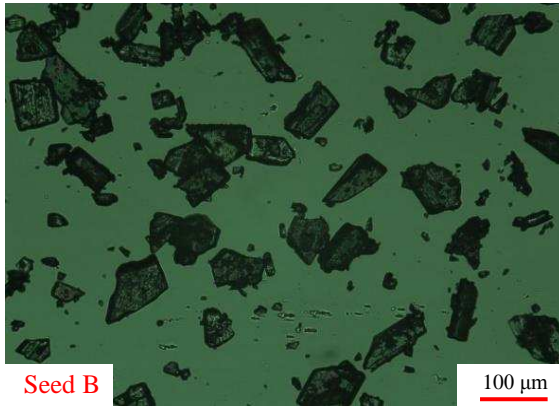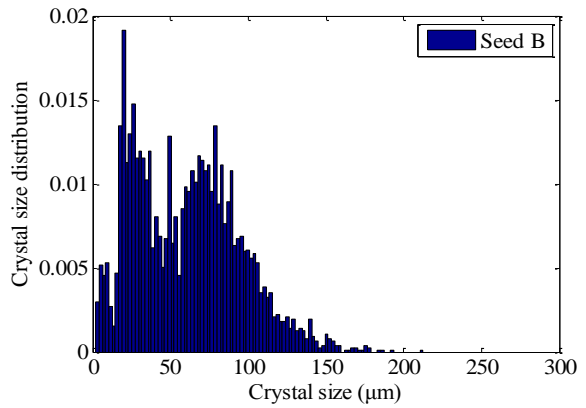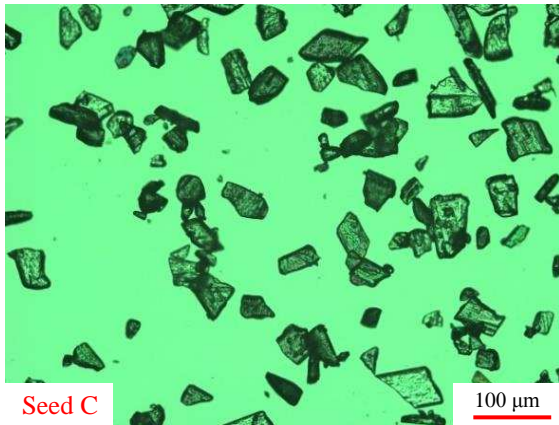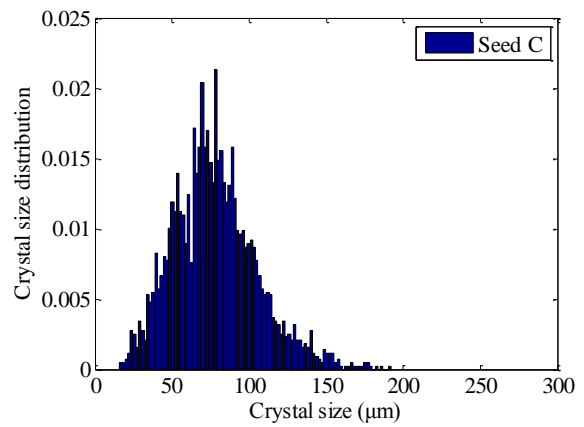
Figure 2. Microscopy images of seeds prepared by three different operating conditions and the corresponding size distributions measured by a non-invasive imaging system: (a) Seed A; (b) Seed B; (c) Seed C; (d) SSD of Seed A; (e) SSD of Seed B; (f) SSD of Seed C.
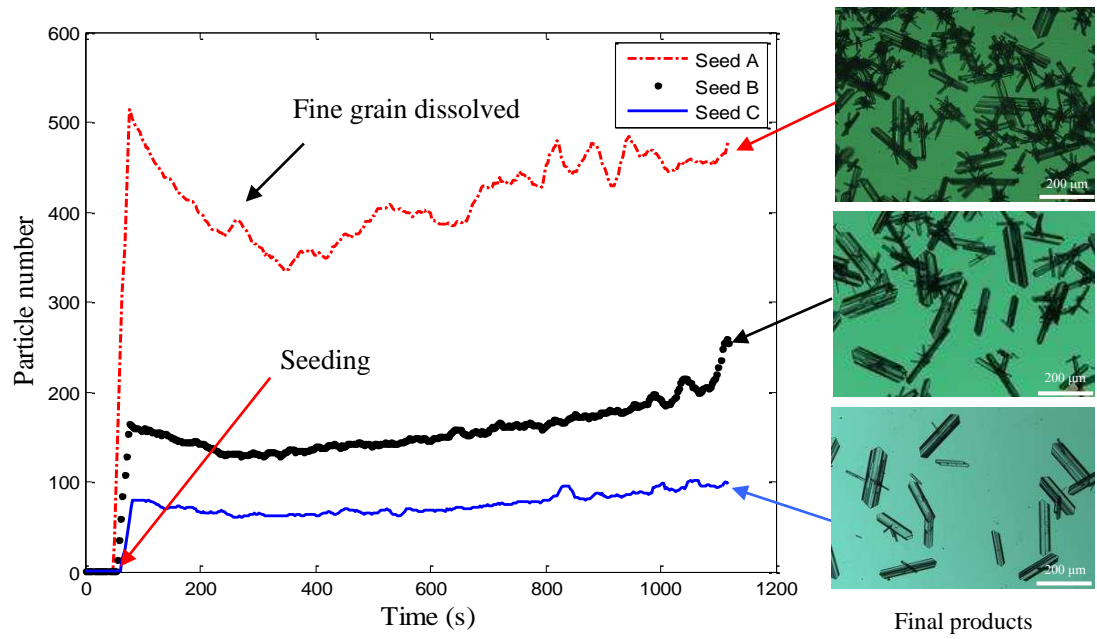
Figure 3. Evolution of the particle number using different seeds for crystallization along with microscopy images of final products.
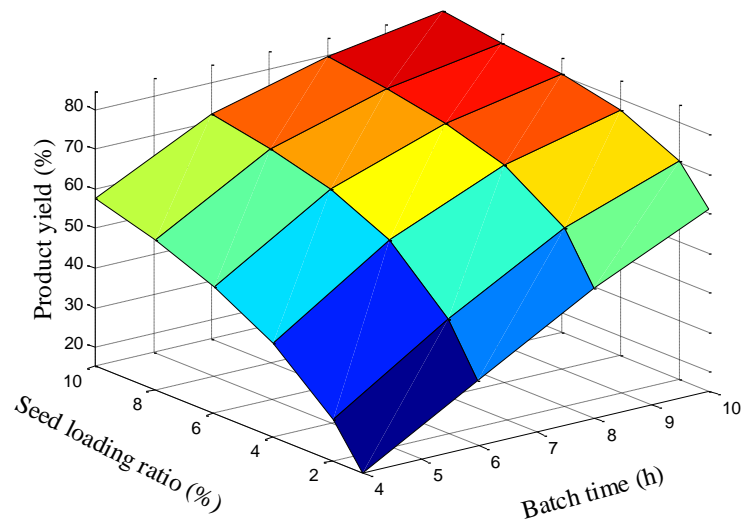


Figure 4. Product yield with respect to SLR and batch time in terms of SSD ~N (40, 15).
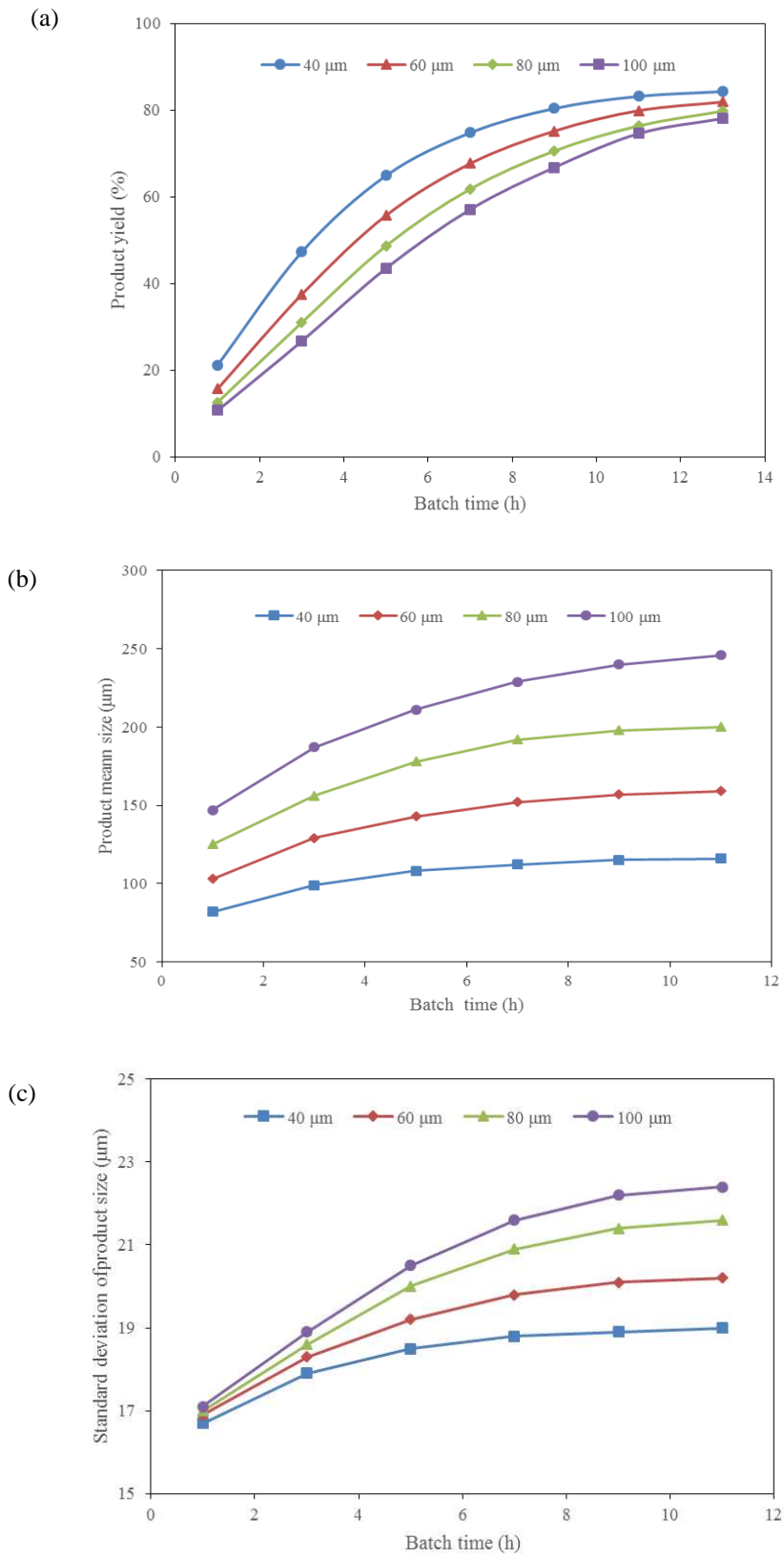
Figure 5. Effect of SMS on the product attributes: (a) PY; (b) PMS; (c) SDPS.

(a)

(b)
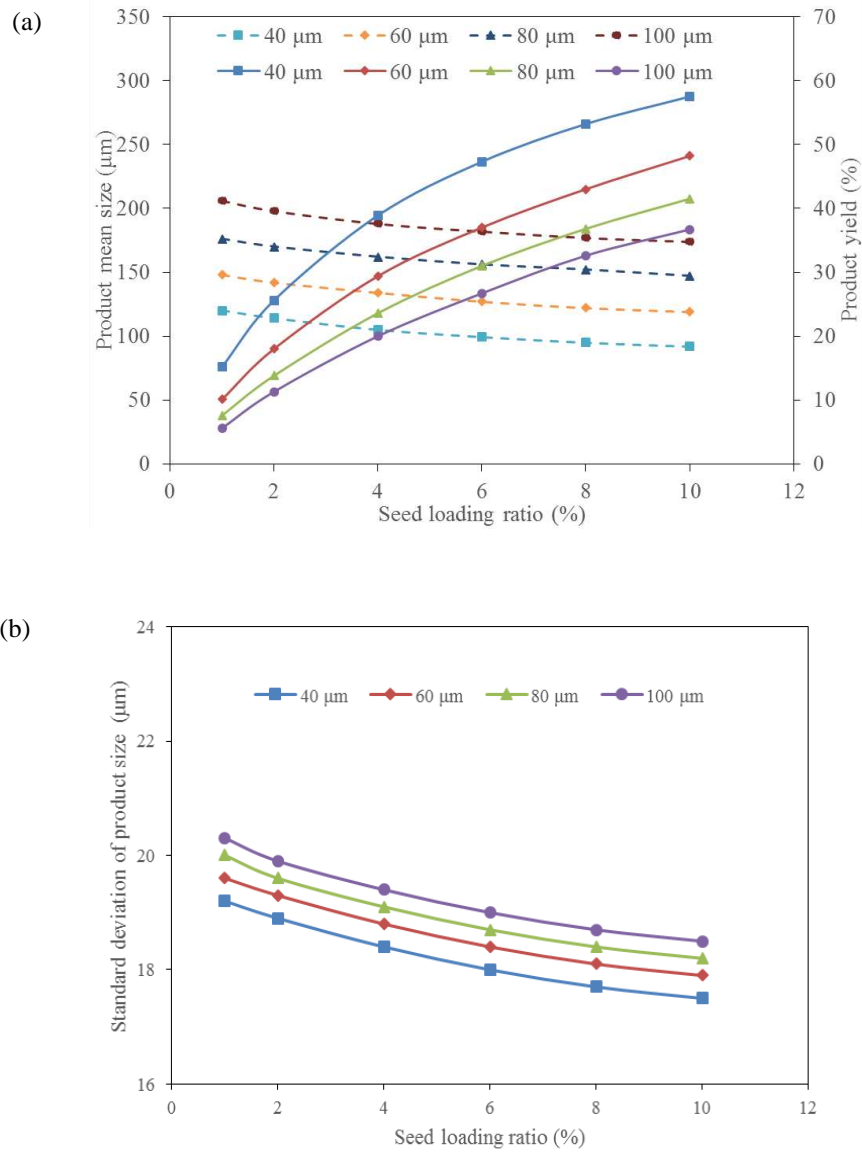
Figure 6. Cross effect of SLR and SMS on the product attributes: (a) PY and PMS; (b) SDPS.

(a)

(b)
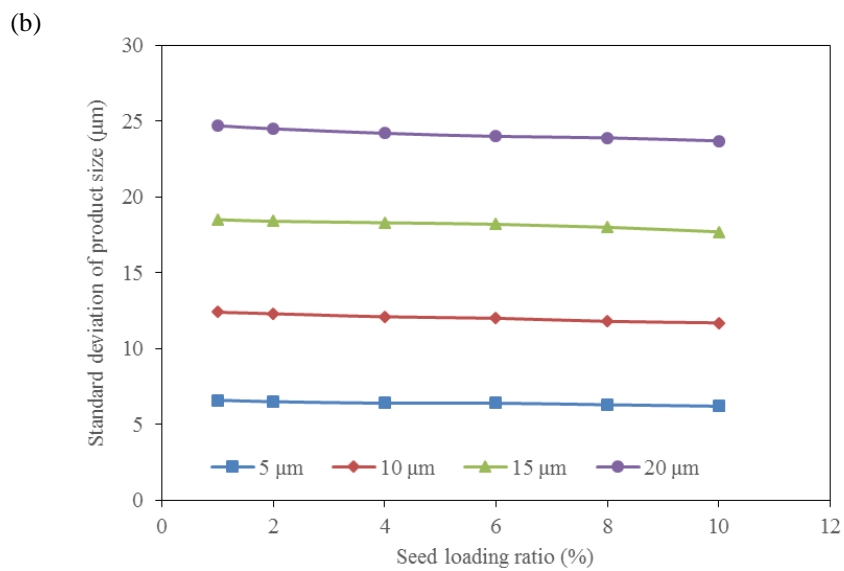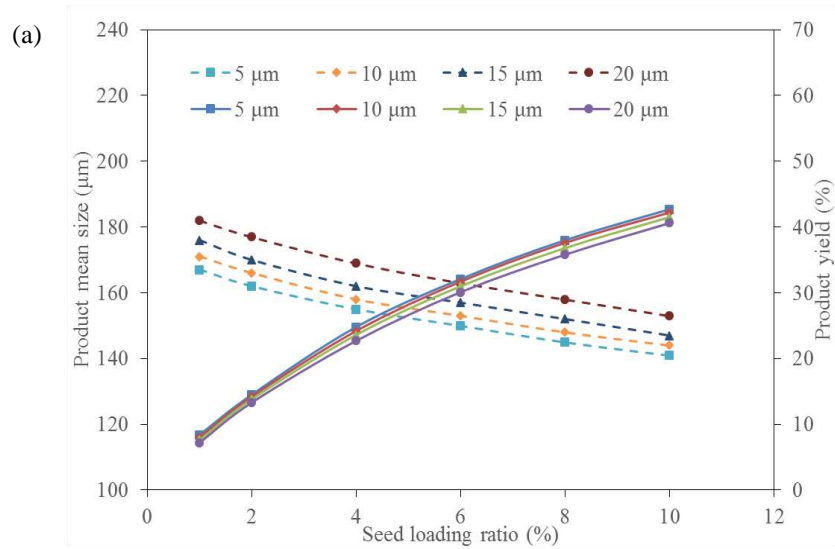
Figure 7. Cross effect of SLR and SDSS on the product attributes: (a) PY and PMS; (b) SDPS.
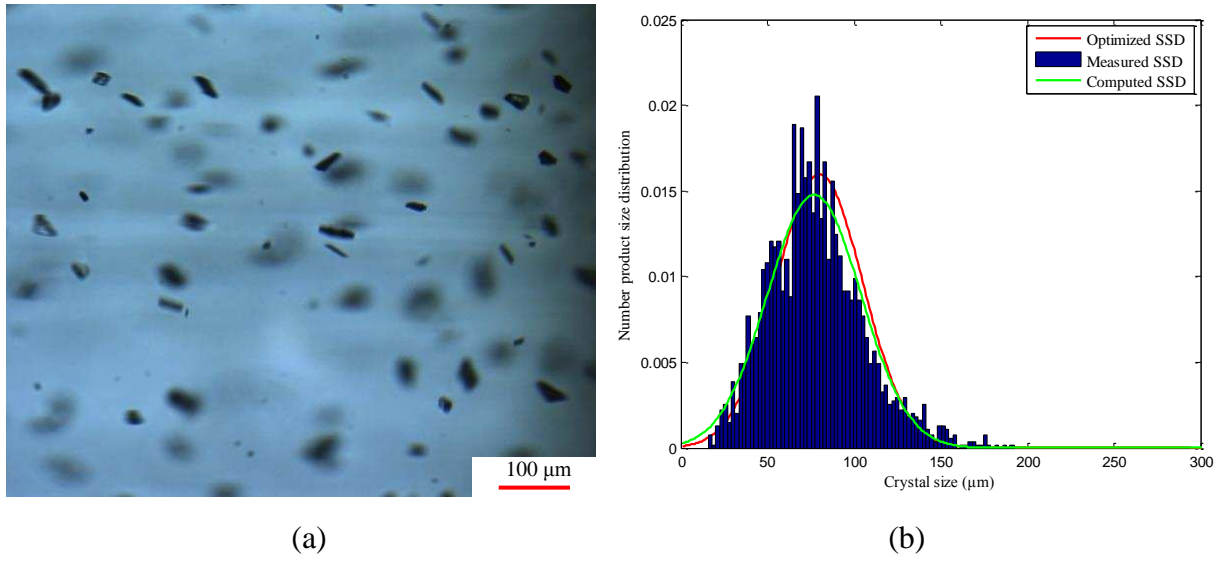
Figure 8. Illustration of the prepared crystal seeds: (a) snapshot by an in-situ imaging system;

(b) comparison of the measured SSD with the optimized SSD by simulation.
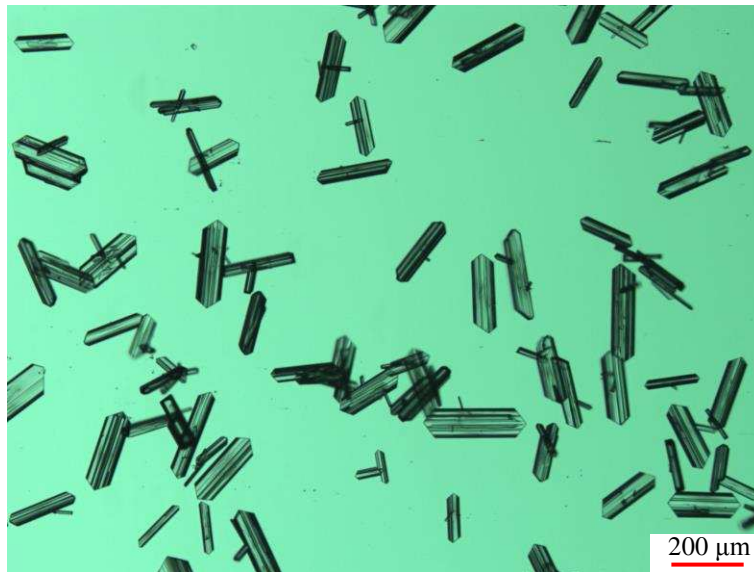


Figure 9. Microscopy image of the final products.
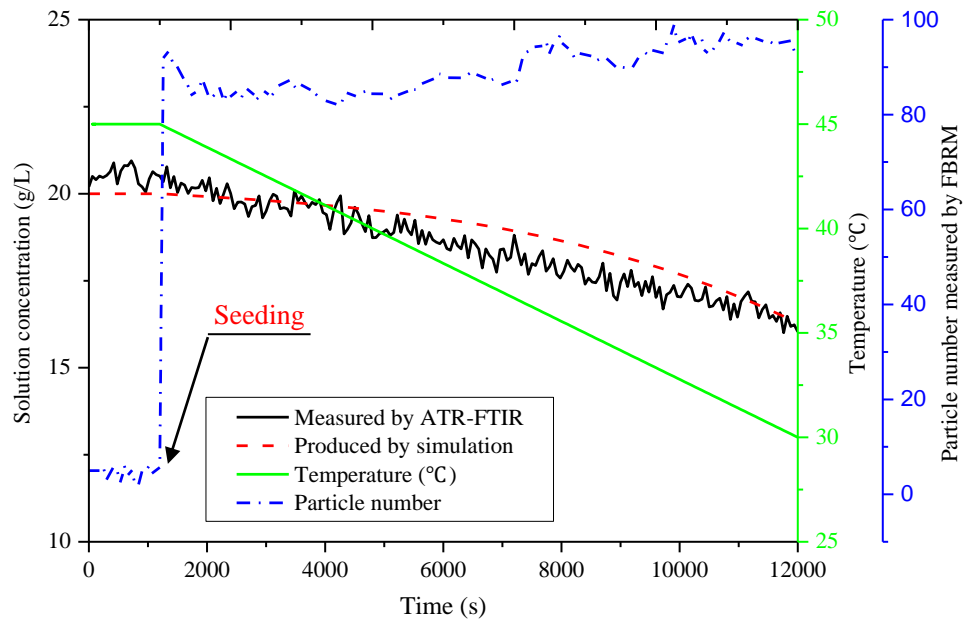
Figure 10. Comparison of the measured solution concentration during crystallization and the simulation result



(a)



(b)
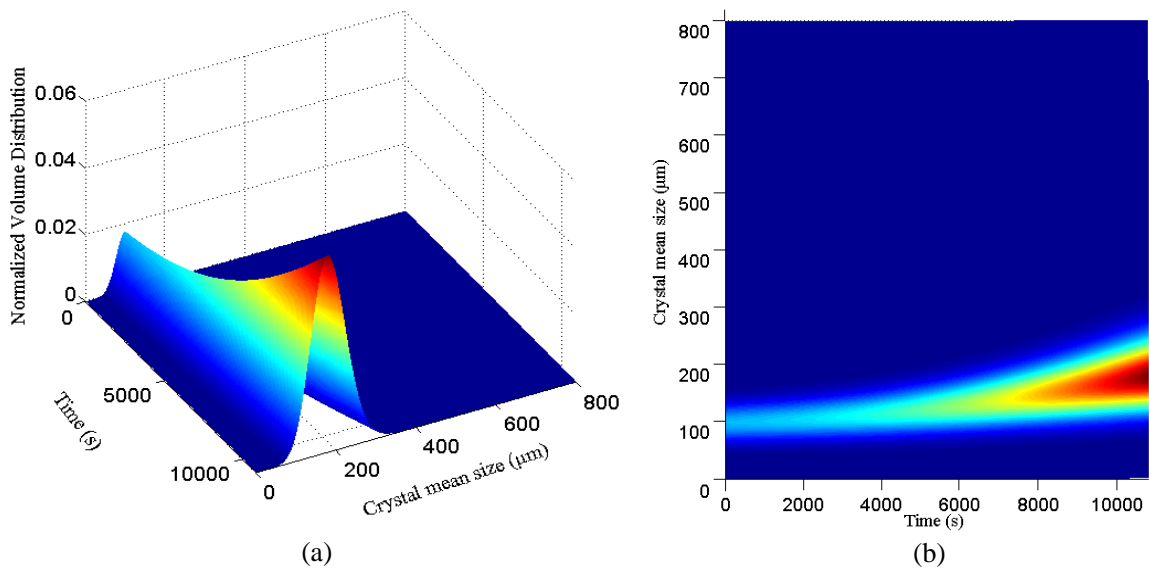
Figure 11. Dynamic evolution of the simulation model based on the optimized seed recipe: (a) CSD; (b) a projection of CSD.
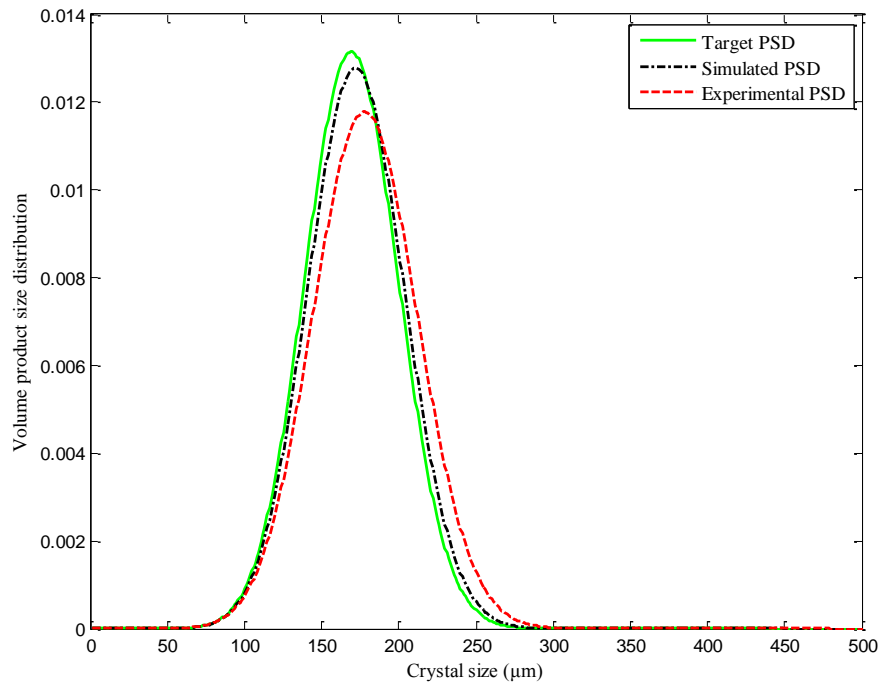
Figure 12. Comparison between the target and measured PSDs in terms of volume percentages of different sizes of final products.